Molecular Vision 2015; 21:347-359 <http://www.molvis.org/molvis/v21/347>
Received 20 January 2015 | Accepted 30 March 2015 | Published 1 April 2015

Bestrophin-1 influences transepithelial electrical properties and Ca^{2+} signaling in human retinal pigment epithelium

Alan D. Marmorstein,[1] Tyson R. Kinnick,[2] J. Brett Stanton,[2] Adiv A. Johnson,[1] Ronald M. Lynch,[2] Lihua Y. Marmorstein[1]

[1]Department of Ophthalmology, Mayo Clinic, Rochester, MN; [2]Department of Physiology, University of Arizona, Tucson, AZ

Purpose: Mutations in *BEST1*, encoding Bestrophin-1 (Best1), cause Best vitelliform macular dystrophy (BVMD) and other inherited retinal degenerative diseases. Best1 is an integral membrane protein localized to the basolateral plasma membrane of the retinal pigment epithelium (RPE). Data from numerous in vitro and in vivo models have demonstrated that Best1 regulates intracellular Ca^{2+} levels. Although it is known from in vitro and crystal structure data that Best1 is also a calcium-activated anion channel, evidence for Best1 functioning as a channel in human RPE is lacking. To assess Best1-associated channel activity in the RPE, we examined the transepithelial electrical properties of fetal human RPE (fhRPE) cells, which express endogenous Best1.

Methods: Using adenovirus-mediated gene transfer, we overexpressed Best1 and the BVMD mutant $Best1^{W93C}$ in fhRPE cells and assessed resting transepithelial potential (TEP), transepithelial resistance, short circuit current (I_{sc}), and intracellular Ca^{2+} levels. Cl^- currents were directly measured in transfected HEK293 cells using whole-cell patch clamp.

Results: $Best1^{W93C}$ showed ablated Cl^- currents and, when co-expressed, suppressed the channel activity of Best1 in HEK293 cells. In fhRPE, overexpression of Best1 increased TEP and I_{sc}, while $Best1^{W93C}$ diminished TEP and I_{sc}. Substitution of Cl^- in the bath media resulted in a significant reduction of I_{sc} in monolayers overexpressing Best1, but no significant I_{sc} change in monolayers expressing $Best1^{W93C}$. We removed Ca^{2+} as a limit on transepithelial electrical properties by treating cells with ionomycin, and found that changes in I_{sc} and TEP for monolayers expressing Best1 were absent in monolayers expressing $Best1^{W93C}$. Similarly, inhibition of calcium-activated anion channels with niflumic acid reduced both I_{sc} and TEP of control and Best1 monolayers, but did not notably affect $Best1^{W93C}$ monolayers. Stimulation with extracellular ATP induced an increase in TEP in control monolayers that was greater than that observed in those expressing $Best1^{W93C}$. Examination of $[Ca^{2+}]_i$ following ATP stimulation demonstrated that the expression of $Best1^{W93C}$ impaired intracellular Ca^{2+} signaling.

Conclusions: These data indicate that Best1 activity strongly influences electrophysiology and Ca^{2+} signaling in RPE cells, and that a common BVMD mutation disrupts both of these parameters. Our findings support the hypothesis that Best1 functions as an anion channel in human RPE.

The bestrophinopathies are a collection of five diseases causally associated with mutations in the gene *BEST1* (BEST1 database). The most common bestrophinopathy is Best vitelliform macular dystrophy (BVMD, OMIM 153700), a retinal disease characterized by an autosomal dominant mode of inheritance, an accumulation of lipofuscin in the retinal pigment epithelium (RPE), the formation of macular lesions, and vision loss [1-4]. *BEST1* encodes the protein bestrophin-1 (Best1), a homo-pentameric anion channel [5,6] and integral membrane protein that is localized to the basolateral plasma membrane of the RPE [7,8]. Best1 has also been reported in the cytosolic compartment adjacent to the basolateral plasma membrane [9-12], where it may regulate Ca^{2+} stores by conducting anions as a counter to Ca^{2+} [9-11].

Correspondence to: Alan D. Marmorstein, Department of Ophthalmology, Mayo Clinic, 200 1st Street SW, Guggenheim Building, Room 929, Rochester, MN, 55905; Phone: (507) 284-2261 FAX: (507) 284-5866; email: Marmorstein.Alan@mayo.edu

Prior to the identification of the *BEST1* gene, the only fully penetrant symptom of BVMD was considered a reduced electrooculogram (EOG) light peak (LP) with a normal clinical electroretinogram [1-3,13]. The LP is recorded as a change in the corneo-retinal standing potential of the eye. This change in trans-tissue potential is the result of a depolarization of the basolateral plasma membrane of the RPE, and correlates with a change in the transepithelial electrical potential (TEP) of the RPE [14-16]. The change in TEP that is recorded is the LP and is believed to be generated by a Ca^{2+}-dependent Cl^- conductance across the basolateral plasma membrane of the RPE [14-16], where Best1 is localized [7].

Whole-cell patch clamp analysis of Best1 and other bestrophins in heterologous systems demonstrates that they function as Ca^{2+}-activated anion channels (CAAC), and that disease-causing mutations in *BEST1* impair anion channel activity [17-19]. This led to the hypothesis that the diminished EOG characteristic of BVMD was due to a loss of Best1 CAAC activity. However, our prior studies using a whole-cell

patch clamp on RPE from *Best1* knock-in and knockout mice failed to find any effect of either the absence of Best1 or the Best1 mutation W93C on Ca^{2+}-activated Cl^- conductances in RPE cells isolated from those mice [20,21]. Furthermore, we have shown that the LP is not generated by Best1, but is regulated by it [20]. Although it is known from in vitro data [17-19], crystal structure data [5,6], and in vivo neuronal data [22,23] that Best1 is an anion channel, Best1 anion channel activity in the RPE of any species has yet to be documented.

Best1 also serves as a regulator of intracellular Ca^{2+} levels. We and others have shown that, in vitro, Best1 regulates the activation/inactivation kinetics of voltage-dependent Ca^{2+} channels (VDCCs) [20,24,25], that it physically interacts with VDCC subunits [25-27], and that Best1 mutants alter the functional interaction of Best1 and VDCCs [24,28]. In Best1-deficient mice, we have shown that stimulation of the RPE with ATP, a candidate light peak substance [29], results in increased $[Ca^{2+}]_i$ in comparison with wild-type (WT) mice. Best1-deficient mice also exhibit a more robust LP luminance response than WT mice [20]. Conversely, mice harboring the BVMD-associated W93C mutation in Best1 exhibit a LP luminance response reminiscent of VDCC-deficient mice [21]. Interestingly, the LP is diminished by inhibition of VDCCs [30], and the LP luminance response is desensitized and diminished in mice lacking either the $Ca_v1.3$ [30] or B_4 [20] subunits of VDCCs. Best1 has also been reported to regulate Ca^{2+} stores in RPE [9-11]. Thus, defective Ca^{2+} signaling and/or Ca^{2+} store release may underlie the LP defect in BVMD. This could occur either indirectly via its channel activity or directly via its regulation of VDCCs. Although the latter function remains to be validated in vivo, RPE cells from $Best1^{W93C}$ knock-in mice exhibit no detectable Ca^{2+} release following ATP stimulation [21].

Based on these observations, we sought to examine the effects of Best1 on transepithelial electrical properties and intracellular Ca^{2+} signaling in human RPE. To accomplish this, we studied Best1 and the BVMD-associated mutant $Best1^{W93C}$ using cultured fetal human RPE (fhRPE) monolayers. $Best1^{W93C}$ was chosen because we have previously established using mouse and rat models that this mutant diminishes the LP response [21,31]. We have also shown that $Best1^{W93C}$ disrupts the functional interaction of Best1 with VDCCs in a heterologous system [24] and physically interacts with WT Best1 [32], consistent with the dominant nature of BVMD. W93C is also one of the most frequently described mutations associated with BVMD. In contrast to other RPE culture models (e.g., ARPE-19, D407, RPE-J), fhRPE expresses endogenous human Best1 (hBest1) [32,33], mimics many of the ion transport properties of RPE in the eye [33], and generates a high enough transepithelial resistance (TER) to permit studies of transepithelial ion flux [33,34]. This is the first manuscript to investigate the effects of Best1 on transepithelial electrophysiology in human RPE. Our studies lead us to conclude that Best1 activity regulates both transepithelial electrical properties and Ca^{2+} signaling of RPE, and that disruption of both functions of Best1 may contribute to the pathogenesis of BVMD.

METHODS

Cell culture, adenovirus-mediated gene transfer, and transfection: Cultures of fhRPE, established as described by Hu and Bok [33], were maintained as before [32]. For experiments, fhRPE cells were plated on poly-L-lysine–coated glass coverslips, 96-well plates, or laminin-coated 0.4 µm pore size Millicell-HA filters (12-mm; Millipore, Bedford, MA) at 2.5×10^5 cells/cm^2 in Chee's essential medium, containing 1.8 mM Ca^{2+}, 1% bovine retinal extract, and 1% FBS. Monolayers were differentiated for a period of ≥ 8 weeks before use in any experiments. Expression of hBest1 or $hBest1^{W93C}$ was accomplished using replication defective adenovirus vectors at an MOI of 3, as described elsewhere [7,32]. Controls were performed using adenovirus-mediated gene transfer with an empty "null" viral vector.

Immunofluorescence: Immunofluorescence staining of hBest1 in fhRPE was performed as described previously [32]. In brief, fhRPE grown on Millicell HA filters were stained for hBest1 using the previously described antibody E6–6 [7]. Nuclei were stained using 4′,6-diamidino-2-phenylindole (DAPI; Life Technologies, Carlsbad, CA) for positional referencing. Images in the X-Y and X-Z planes were obtained using a Leica SP5 confocal microscope with a 40X oil immersion objective. Images were procured and processed using Leica's LAS AF Lite software.

Whole-cell patch clamp: WT or mutant hBest1 fused at the C-terminus to enhanced yellow fluorescent protein (eYFP, Invitrogen, Grand Island, NY) or enhanced cyan fluorescent protein (eCFP, Invitrogen, Grand Island, NY) were transfected into HEK293 cells as described previously [32,35]. Single cells identified by CFP or YFP fluorescence were used for whole-cell patch clamp experiments within 48 h. Transfected HEK293 cells were recorded using a conventional whole-cell patch-clamp technique with an EPC-10 amplifier and Patchmaster software (HEKA, Bellmore, NY). Fire-polished borosilicate glass patch pipettes were 3–5 MΩ. Experiments were conducted at RT (20–24 °C). Since the liquid junction potentials were small (<2 mV), no correction was made. The high Ca^{2+} intracellular solution contained (mM): 146 CsCl, 2 $MgCl_2$, 5 Ca^{2+}-EGTA (free Ca^{2+} □20 µM),

10 HEPES, 10 sucrose, pH 7.3, adjusted with NMDG. The standard extracellular solution contained (mM): 140 NaCl, 5 KCl, 2 $CaCl_2$, 1 $MgCl_2$, 15 glucose, 10 HEPES, pH 7.4 with NaOH. This combination of intracellular and extracellular solutions set E_{rev} for Cl^- currents to zero, while cation currents carried by Na^+ or Cs^+ had very positive or negative E_{rev}, respectively. Osmolarity was adjusted with sucrose to 303 mOsm for all solutions.

Epithelial electrophysiology: All experiments were performed in a water jacketed Ussing chamber similar to that described by Oakley et al. [36] and Miller and Steinberg [37]. The chamber was modified to hold Millicell HA cell culture inserts and to contain larger bath volumes (8.5 ml apical, 8.0 ml basal). All experiments began by perfusing both sides of the chamber at a rate of 7 ml/min with Ringers solution containing in (mM): 113.4 NaCl, 5 KCl, 5.6 glucose, 0.8 $MgCl_2$, 2 glutathione, 1.8 $CaCl_2$, and 26.2 $NaHCO_3$, pH 7.4, until the TEP stabilized. All solutions were constantly gassed with 95% O_2, 5% CO_2. For the Cl^- ion-substitution experiments, 90% of the normal Cl^- content in both the apical and basal baths was replaced by gluconate [in (mM): 108.9 D-gluconic acid (Na^+ salt), 4.5 NaCl, 5 KCl, 5.6 glucose, 0.8 $MgCl_2$, 2 glutathione, 1.8 $CaCl_2$, and 26.2 $NaHCO_3$, pH 7.4]. For experiments examining Ca^{2+} effects, monolayers were stimulated with 500 nM ionomycin and 100 µM niflumic acid (NFA). Ionomycin was added to both the apical and basal baths, while NFA was added only to the basal bath.

Voltage across fhRPE monolayers or the TEP was recorded using Ag/AgCl pellet electrodes bridged with agar 0.5 M KCl bridges in each bath. Signals were passed through a low-pass Bessel filter, amplified using a DP-304 Differential Amplifier (Warner Instruments, Inc., Hamden, CT), digitized, and recorded and analyzed on a Dell PC using LabScribe 1.821 software (iWorx, Dover, NH). The TER of the monolayers was determined by passing bipolar 10 µA pulses (DS8000 Digital Stimulator, World Precision Instruments, Inc., Sarasota, FL) across the monolayer every 30 s between Ag-AgCl pellets placed in each bath. TER was measured from the current-induced voltage changes across the monolayer. Short circuit current (I_{sc}) was calculated as I_{sc}=(TEP/TER).

Ca^{2+} measurements: fhRPE were grown on glass coverslips or in 96-well cell culture plates. Overexpression of hBest1 or hBest1 mutants was achieved by adenovirus transduction as described above and in previous work [32], with a null vector serving as a control.

For Ca^{2+} concentration measurements, cells on coverslips were loaded with the Ca^{2+} indicator dye FURA-2 AM 48 h following infection. Coverslips were then secured in a perfusion chamber on the stage of a Nikon TE200 inverted microscope with a xenon light source. The chamber was continuously perfused with CO_2/HCO_3^- containing Ringers solution (see above) warmed to 37 °C by an in-line heater. FURA-2 AM fluorescence was excited sequentially with 340 nm and 380 nm light and acquired with a 515 / 70 nm band pass filter and 40X air or oil objective using a Cascade 512b cooled CCD camera (Photometrics, Tucson, AZ). Data were collected every 5 s and analyzed using MetaFluor Software (Molecular Devices, Sunnyvale, CA) and Excel 2004. $[Ca^{2+}]_i$ was determined as follows: The ratios of the intensity of emissions at 340 nm / 380 nm was determined for each individual cell in a field. Absolute values of $[Ca^{2+}]_i$ were estimated as before [20,21] according to Grynkiewicz et al. [38], using a bath solution with 10 µM ionomycin to saturate Fura-2 with Ca^{2+} and Ca^{2+}-free bath solution with 10 µM ionomycin to deplete Fura-2 from Ca^{2+}. Resting $[Ca^{2+}]_i$ was determined from the average $[Ca^{2+}]_i$ of all cells in a field recorded for 3 min before addition of a stimulus.

To evaluate changes in $[Ca^{2+}]_i$ in response to varying doses of ATP, cells grown on 96-well plates were loaded with a proprietary Ca^{2+} sensitive fluorescent indicator using the Calcium 4 Assay Kit (Molecular Devices, Sunnydale, CA) according to the manufacturer's instructions. The cells were then placed in a Flexstation 3 (Molecular Devices) and imaged using 485 nm excitation/525±10 nm emissions. A 90 s baseline was established, after which ATP was added to the solutions and the responses recorded every 3 s for an additional 5 min. Data were acquired using SOFTmax Pro v5.2 software (Molecular Devices). Changes in cell Ca^{2+} were evaluated by normalizing fluorescence intensity levels to that measured immediately preceding the addition of ATP. Following the experiment, hBest1 expression was verified by immunoprecipitation with anti-Best1 pAb-125, and western blotting with anti-Best1 maB E6–6, as previously described [7].

Statistics: Statistics were done using ANOVA (ANOVA) and *t* tests. Significance was defined as $p<0.05$.

RESULTS

hBest1^{W93C} impairs anion channel activity: To date, all disease-causing mutants of hBest1 tested have exhibited diminished anion channel activity [17,18]. We confirmed this for hBest1^{W93C} by performing a whole-cell patch clamp of HEK293 cells heterologously expressing hBest1 fused with YFP or CFP (Best1-YFP, Best1-CFP), Best1^{W93C}-YFP, or YFP alone. We have previously shown that the addition of a CFP or YFP tag to the C-terminus of hBest1 does not mitigate its ability to function as an anion channel [35]. As

shown in Figure 1A, Best1-YFP and Best1-CFP produce significant Cl^- currents, which are nearly absent from control cells. Cells transfected with Best1-YFP and Best1-CFP produced currents with amplitudes between those of Best1-YFP and Best1-CFP (Figure 1A). In contrast, Best1^{W93C}-YFP produced little current in comparison to Best1-YFP (Figure 1B). In cells expressing both Best1^{W93C}-YFP and Best1-CFP, Cl^- currents were substantially diminished relative to cells expressing Best1-YFP and Best1-CFP (Figure 1C). This is the first time that differently tagged forms of fluorescent Best1 have been co-expressed together for whole-cell patch-clamp analysis, and the first time that such an analysis was done where WT and mutant Best1 could both be confirmed to be co-expressed. This is particularly significant, as it was not uncommon to observe cells in co-transfected populations only expressing one of the two Best1 variants (e.g., Best1^{W93C}-YFP only or Best1-CFP only).

Effects of hBest1 and hBest1^{W93C} on transepithelial electrical properties: As we have done in previous work [32], primary cultures of fhRPE were grown on permeable supports. These cells produce monolayer cultures that normally express hBest1 (Figure 2A,B) and can generate a TER of >400 Ω x cm^2 (Figure 3B) [33,34] when measured in Ringer's solution. hBest1 and hBest1^{W93C} were overexpressed in the monolayers using adenovirus mediated gene transfer. Controls were performed using adenovirus-mediated gene transfer with an empty "null" viral vector. We have previously demonstrated that adenovirus-mediated gene transfer causes overexpression of these proteins in fhRPE cells relative to endogenous levels of Best1 [32]. Localization of overexpressed hBest1 and hBest1^{W93C} was previously observed to be to the basolateral plasma membrane in fhRPE cells [32] and the RPE of rat eyes [31]. We confirm this here by showing immunofluorescence and confocal microscopy of endogenous Best1 (Figure 2A,B), overexpressed hBest1 (Figure 2C,D), and overexpressed hBest1^{W93C} (Figure 2E,F).

Overexpression of hBest1 or hBest1^{W93C} did not affect TER (Figure 3B) when compared to control monolayers transduced with a null adenovirus vector. Monolayers overexpressing hBest1 exhibited a significant ($p<0.05$) increase in TEP (Figure 3A) and the calculated short circuit current (I_{sc}, Figure 3C), while monolayers expressing hBest1^{W93C} exhibited a significantly diminished TEP (Figure 3A) and I_{sc} (Figure 3C).

To test whether the changes in I_{sc} in cells overexpressing hBest1 and hBest1^{W93C} were due in part to an altered Cl^- conductance, 90% of the Cl^- in the apical and basal baths was substituted with gluconate. The addition of hBest1 anion channels to the basolateral membrane would theoretically increase electrogenic Cl^- flux and therefore account for the observed increase in I_{sc} (Figure 3C). Removing bath Cl^- would inhibit Cl^- uptake by the apical Na^+-K^+-Cl^- co-transporter and therefore serve as an indirect test of the basolateral Cl^- flux contributing to this observed change in I_{sc}. Substitution resulted in observable voltage changes (Figure 3D) in all monolayers. However, statistically significant changes in I_{sc} (Figure 3E) were observed only in monolayers overexpressing hBest1, which showed a significant reduction in I_{sc} following

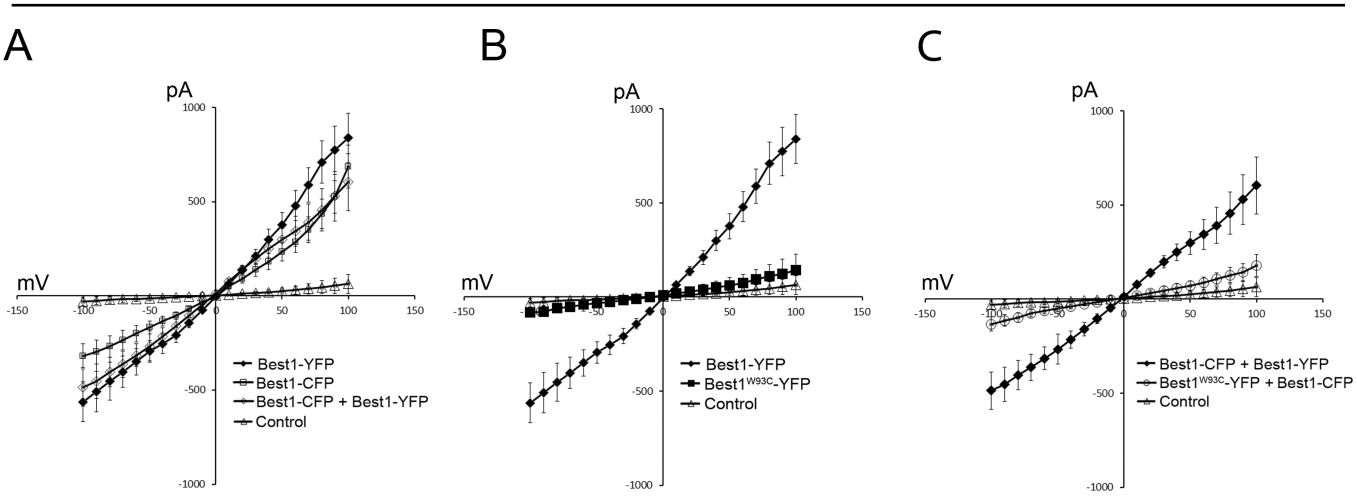

Figure 1. Whole-cell chloride currents mediated by Best1-CFP, Best1-YFP, and Best1^{W93C}-YFP. **A**: Whole-cell patch-clamp recordings were performed on HEK293 cells transfected with Best1-CFP, Best1-YFP, or Best1-CFP and Best1-YFP. Cells expressing fluorescently tagged Best1 exhibited robust chloride currents compared to untransfected cells recorded from the same plate. **B**: In contrast, Best1^{W93C} exhibited a significant loss of anion channel activity compared to Best1-YFP (**B**), and dominantly inhibited the anion channel activity of wild-type Best1-YFP when co-expressed (**C**).

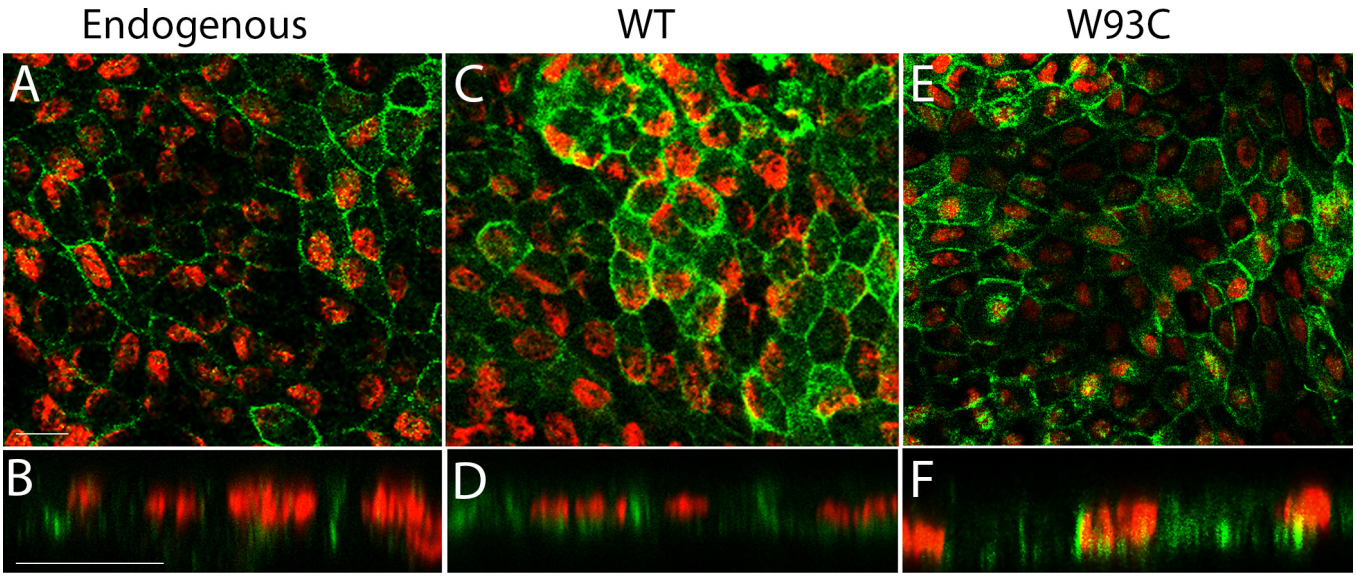

Figure 2. Localization of endogenous hBest1, overexpressed hBest1, and overexpressed hBest1^{W93C} in fhRPE cells. Monolayers of fhRPE were stained for hBest1 expression (green) and examined by confocal microscopy in the X-Y (**A**, **C**, **E**) and X-Z (**B**, **D**, **F**) planes. Endogenous hBest1 (**A**, **B**) was observed to be localized to the basolateral plasma membrane, as was hBest1 in monolayers overexpressing hBest1 (**C**, **D**) or hBest1^{W93C} (**E**, **F**). Nuclei (red) were stained for positional referencing. Scale bars: 20 µM.

substitution with gluconate. This change in I_{sc} was reversible, as it returned to its previous value after restoring Cl^- to the bath media (Figure 3E).

Effects of hBest1 and hBest1^{W93C} on transepithelial electrical properties following application of ionomycin: We have previously shown that, following ATP stimulation, Ca^{2+} signaling is suppressed in RPE from mice heterozygous or homozygous for the W93C mutation [21]. To assess whether the diminished TEP (Figure 3A) and I_{sc} (Figure 3C) observed in monolayers overexpressing hBest1^{W93C} was due to altered Ca^{2+} signaling, we eliminated Ca^{2+} influx as a limit by treating monolayer cultures with the Ca^{2+} ionophore ionomycin (Figure 4). This would be predicted to have the effect of overcoming any suppressive effects hBest1 could exert on $[Ca^{2+}]_i$ and, as such, any observed changes would reflect its activity as an anion channel.

In control monolayers, ionomycin treatment resulted in a biphasic increase in TEP above the resting potential (indicated as P0; Figure 4A). The two peaks in TEP stimulated by ionomycin were designated P1 and P2, respectively (Figure 4A). After P2 reached a plateau, the monolayers were treated with NFA, a broad inhibitor of hBest1 and other Ca^{2+}-dependent ion channels. At any point in the time course, there was no significant change in I_{sc} (Figure 4C), TEP (Figure 4D), or TER (Figure 4E) for monolayers expressing hBest1^{W93C}. Compared to control and overexpressing hBest1 monolayers, however, monolayers expressing hBest1^{W93C} exhibited significantly lower ($p<0.05$) TEP and I_{sc} at the P0, P1, P2, and NFA time points (Figure 4C,D). The overall response (Figure 4B) of monolayers overexpressing hBest1 appeared to be similar to controls'. Although the I_{sc} and TEP during the P0 phase were higher in monolayers overexpressing hBest1 compared to controls', the maximum I_{sc}, TEP, and TER at P1 and P2 (Figure 4C,D,E) were nearly identical in controls and monolayers overexpressing hBest1. Moreover, the effect of NFA on these properties in monolayers overexpressing hBest1 was indistinguishable from controls' (Figure 4C,D). While NFA reduced TEP and I_{sc} of control and hBest1-overexpressing monolayers (Figure 4C,D), NFA failed to impact the TEP or I_{sc} of hBest1^{W93C}-expressing monolayers (Figure 4C,D). For control and hBest1-overexpressing monolayers, the differences in TEP and I_{sc} at each time point were significant.

Effects of hBest1 and hBest1^{W93C} on transepithelial electrical properties following stimulation with ATP: We next examined the effects of hBest1 and hBest1^{W93C} overexpression on the responses of fhRPE cells to a physiologic stimulus that would raise $[Ca^{2+}]_i$, extracellular ATP. ATP has been demonstrated to increase intracellular Ca^{2+} in the RPE [29], a response that is impaired in Best1^{W93C} knock-in mice [21]. Furthermore, ATP is a candidate for the LP substance [16] and is known to activate RPE Cl^- conductances [29]. Figure 5 shows that stimulation of control fhRPE monolayers with 50 µM ATP results in a rapid increase in TEP (Figure 5A,B) and a modest but slower decrease in TER (Figure 5C). I_{sc} in control

monolayers was increased, reaching a plateau within 6 min of stimulus (Figure 5D). In contrast, cells overexpressing hBest1 exhibited a rapid decrease in TEP (Figure 5A,B) and TER (Figure 5C), as well as a smaller increase in I_{sc} compared to controls (Figure 5D). The increase in I_{sc} (Figure 5D) in cells overexpressing hBest1^{W93C} stimulated with extracellular ATP was smaller and slower than both control and hBest1-overexpressing monolayers. This was due primarily to a smaller, slower increase in TEP (Figure 5A,B) in cells overexpressing hBest1^{W93C} compared to controls, although the change in TER (Figure 5C) was comparable. The very large, very rapid decrease in TER (Figure 5C) in monolayers overexpressing hBest1 suggested that the tight junctions of the fhRPE had been compromised. As a result, although we show TEP (Figure 5A,B) and calculated I_{sc} (Figure 5D) for these monolayers, these data cannot be interpreted as representing events occurring at the plasma membrane.

Effects of hBest1 and hBest1^{W93C} on ATP stimulated Ca^{2+} release: The dramatic hBest1- and hBest1^{W93C}-dependent differences observed in fhRPE monolayers in response to ATP motivated us to follow the ATP-induced changes in $[Ca^{2+}]_i$ resulting from hBest1 or hBest1^{W93C} overexpression using the indicator dye fura-2. Mean $[Ca^{2+}]_i$ in fhRPE cells

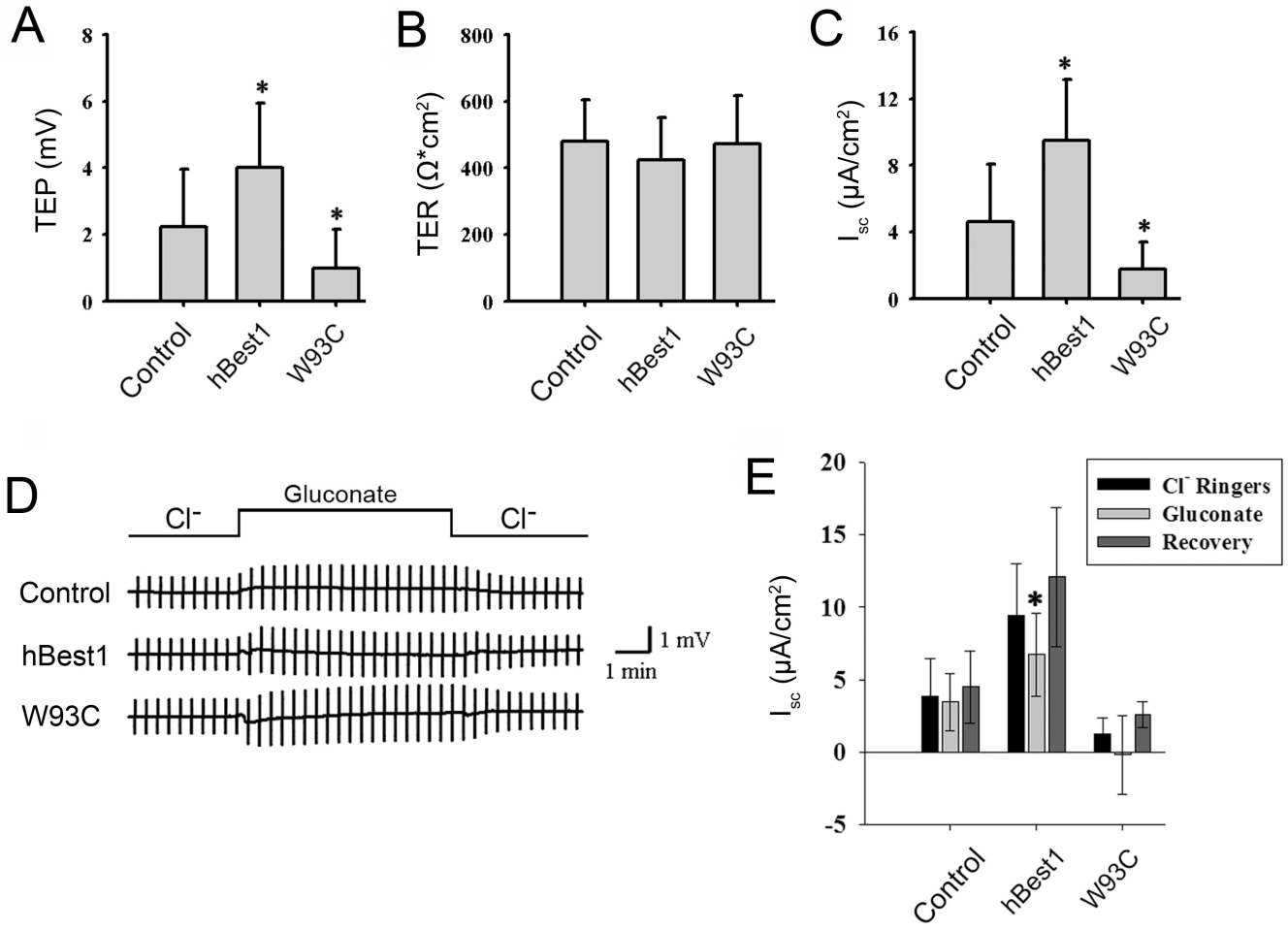

Figure 3. Baseline characteristics of hBest1 and hBest1^{W93C} in fhRPE and the contribution of Cl^- to short circuit current (I_{sc}). The transepithelial electrical properties of monolayers of fhRPE overexpressing hBest1 or hBest1^{W93C} (W93C) were compared with control fhRPE cells. **A**: Transepithelial potential (TEP), (**B**) transepithelial resistance (TER), and (**C**) short-circuit current (I_{sc}) are shown. The contribution of Cl^- to differences in I_{sc} was determined by substitution of Cl^- with gluconate in the bath media. Representative voltage recordings are shown in **D**, and I_{sc} is shown in **E**. Vertical bars in the recordings in **D** represent the voltage change in response to a 10 μA bipolar current pulse used to determine TER at 30 s intervals. For cells overexpressing hBest1, a significant ($p<0.03$) reduction in I_{sc} occurred in response to Cl^- substitution, the effects of which were reversible. Bars in E indicate the I_{sc} recorded in Ringer's (Cl^- Ringers), during ion substitution (gluconate), and following return to Ringer's (recovery). Bars in **A-C** and **E** represent mean ± SD with n=23 control, n=16 hBest1, and n=11 W93C for A-C. For panel **E**, n=20 control, n=14 hBest1, and n=9 W93C. *$p<0.04$ versus control.

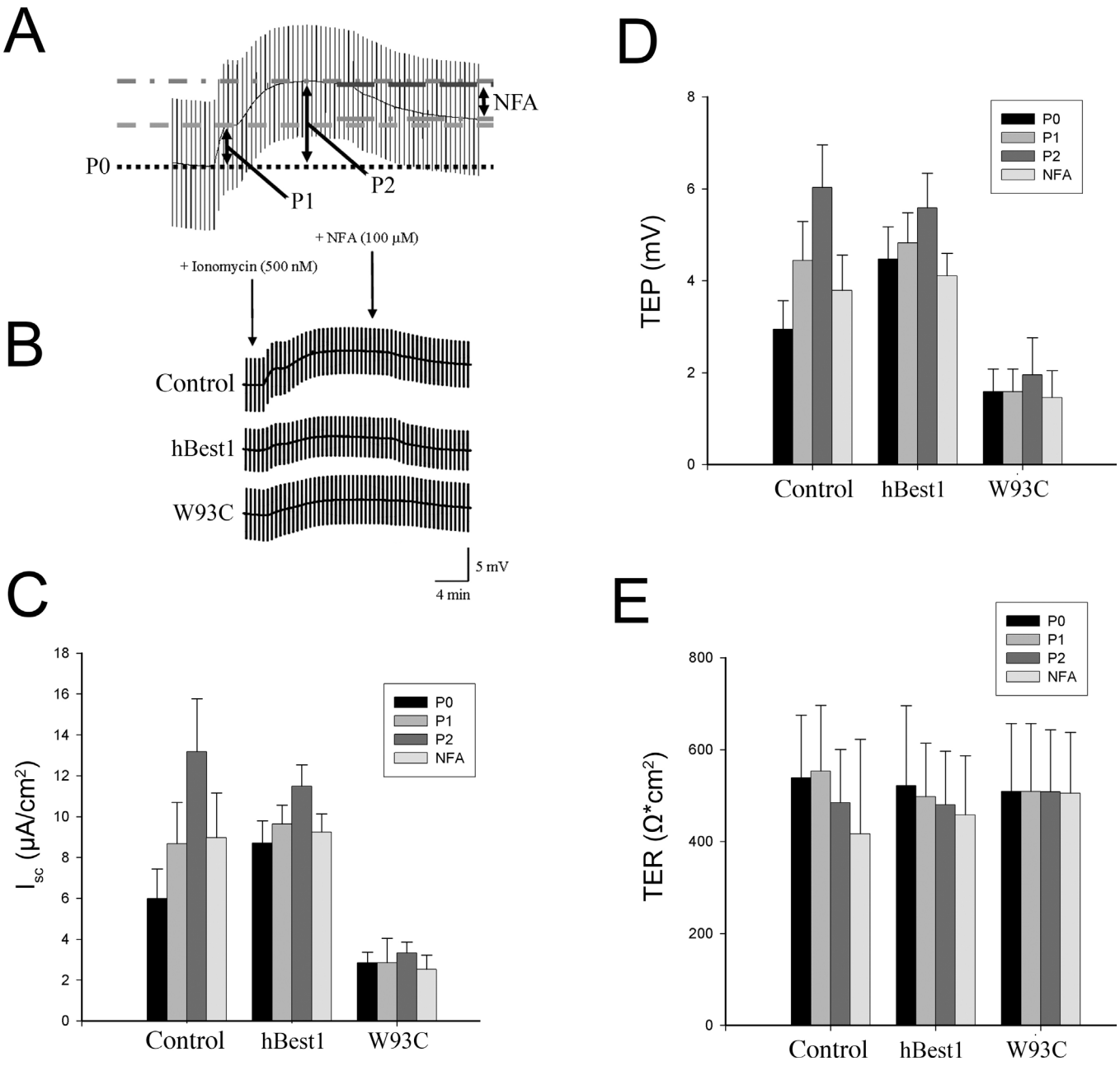

Figure 4. Effect of hBest1 and hBest1^{W93C} expression on Ca^{2+}-stimulated changes in transepithelial electrical properties. **A**: fhRPE cells were treated with 500 nM ionomycin, which caused a biphasic increase in TEP. Each phase of the response was measured at the indicated point. When the TEP reached a plateau, 100 µM NFA was added to the bathing solution to inhibit calcium-activated anion channel activity. Representative recordings of responses are shown in (**B**), demonstrating that overexpression of either hBest1 or hBest1^{W93C} resulted in a suppression of the overall response, and that the response to the addition of NFA was similar in control and monolayers overexpressing hBest1. I_{sc} (**C**) was determined from TEP (**D**) and TER (**E**) for P0, P1, P2, and NFA. Responses were elevated at P0 for hBest1-overexpressing monolayers compared to controls and monolayers overexpressing hBest1^{W93C}. However, at P1, P2, and NFA, I_{sc} was not significantly different between controls and monolayers overexpressing hBest1. Neither ionomycin nor NFA had a significant effect on the transepithelial electrical properties of fhRPE monolayers expressing hBest1^{W93C}. Compared to control and hBest1-overexpressing monolayers, TEP (**D**) and I_{sc} (**C**) were significantly reduced for hBest1^{W93C} monolayers at P0, P1, P2, and NFA. For both control and hBest1-overexpressing monolayers, the differences in TEP (**D**) and I_{sc} (**C**) between different time points were significant ($p<0.05$). Data are mean ± SD, n=9 for control, n=5 for hBest1, and n=6 for W93C.

differed significantly between controls and cells overexpressing hBest1 or hBest1^{W93C}, suggesting that hBest1 can affect resting $[Ca^{2+}]_i$ in human RPE (Figure 6). Compared to controls, mean resting $[Ca^{2+}]_i$ was substantially reduced in monolayers overexpressing hBest1 (Figure 6B). Prior to ATP stimulation, resting $[Ca^{2+}]_i$ was elevated beyond that of controls in monolayers overexpressing hBest1^{W93C} (Figure 6B). Measured resting $[Ca^{2+}]$i was 83±3 nM for controls, 66±11 nM for hBest1, and 90±5 nM for hBest1^{W93C} (average ± SE, n=4 experiments; Figure 6B). Following ATP stimulation, $[Ca^{2+}]_i$ was observed to increase in controls, hBest1-overexpressing cells, and cells expressing hBest1^{W93C} (Figure 6A). However, the increase in mean $[Ca^{2+}]_i$ in cells overexpressing hBest1 was not sustained and $[Ca^{2+}]_i$ returned rapidly to near resting levels. Cells expressing hBest1^{W93C} exhibited an initial fast rise in $[Ca^{2+}]_i$ similar to that observed in hBest1-overexpressing cells, but did not continue to increase and instead remained steady at a level approximately half of that observed in control cells (Figure 6A).

We next examined Ca^{2+} release in fhRPE cells grown in 96-well plates in response to varying doses of ATP. At a dose of 5 µM ATP, controls and cells overexpressing hBest1 exhibited a rapid initial increase in $[Ca^{2+}]_i$ (Figure 7A). However, while $[Ca^{2+}]_i$ levels remained high in control cells, they rapidly returned to near starting levels in cells overexpressing hBest1 (Figure 7A), and the entire response was significantly diminished in monolayers overexpressing hBest1^{W93C} (Figure 7A). To examine this more closely, we generated dose response curves for the initial rise in $[Ca^{2+}]_i$ as a function of ATP concentration. A definitive change in dose response, measured by the initial rise in Ca^{2+}, was noted in cells overexpressing hBest1^{W93C} compared to cells expressing only endogenous hBest1 or cells overexpressing hBest1 (Figure 7B). Analysis of the differences in these responses between groups by ANOVA found them significant ($p<0.003$) for all doses between 1 and 100 µM for hBest1^{W93C} compared to controls.

DISCUSSION

Our data demonstrate that hBest1 influences both transepithelial electrical properties and Ca^{2+} signaling in RPE cells. This is the first study to investigate the effects of Best1 on transepithelial electrical properties in any system, and the first to investigate the effects of hBest1 on Ca^{2+} signaling in fhRPE. We infer a few likely explanations for the mechanisms underlying these changes in fhRPE. The first, which we favor, is that these data provide evidence for hBest1 functioning as a CAAC in human RPE. Recent crystal structure

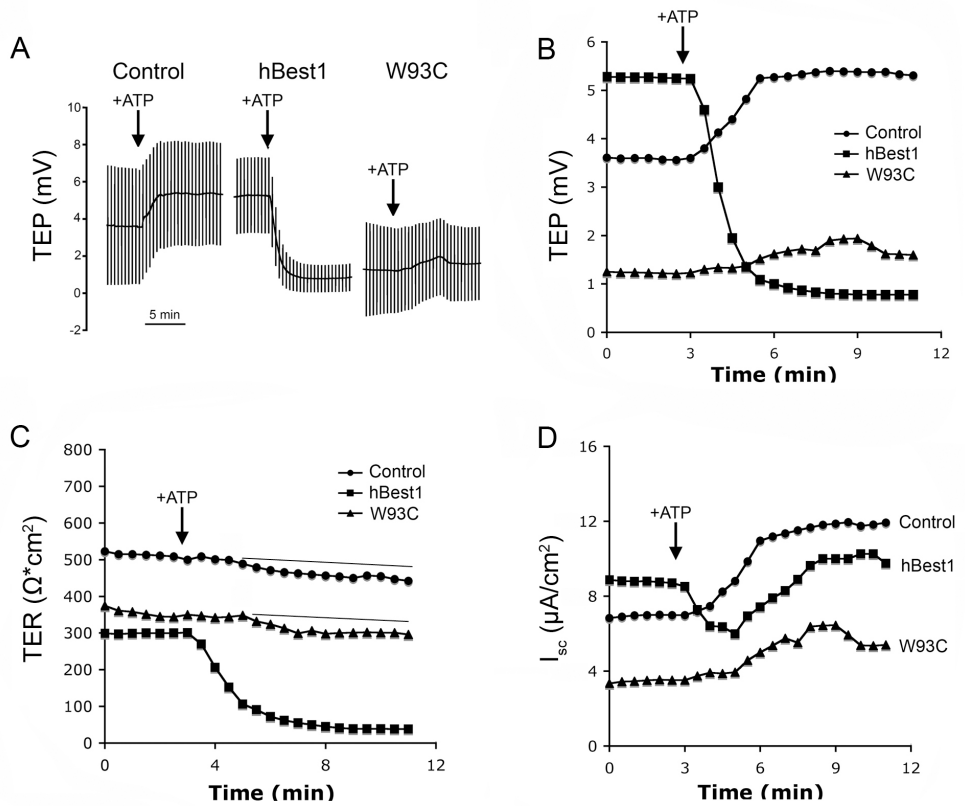

Figure 5. Effect of ATP on transepithelial electrical properties of fhRPE monolayers. Representative recordings from monolayers expressing endogenous hBest1 (control) or overexpressing hBest1 or hBest1^{W93C} (W93C) in response to a 50 µM ATP stimulus are shown in **A**. TEP (**B**) increased in controls and cells expressing hBest1^{W93C} in response to ATP, but diminished significantly in cells overexpressing hBest1. Vertical bars in the recordings in **A** correspond to the voltage deflection induced by a 10 µA bipolar current pulse used to determine TER (**C**), which diminished precipitously in monolayers overexpressing hBest1. I_{sc} (**D**) was calculated from TEP and TER. Data are representative of ≥4 experiments.

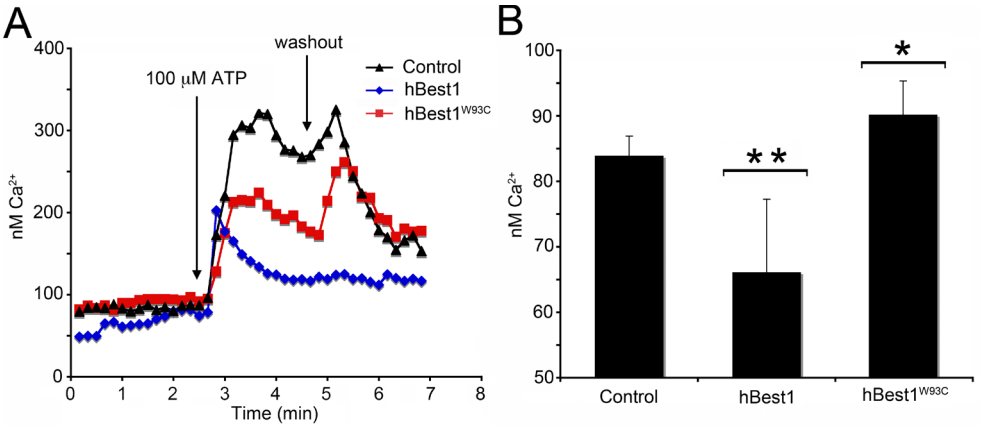

Figure 6. Effect of hBest1 and hBest1^{W93C} on ATP-induced release of Ca^{2+} stores. **A**: The concentration of intracellular Ca^{2+} was measured using the indicator dye fura-2 in fhRPE following stimulation with 100 µM ATP. $[Ca^{2+}]_i$ was compared between control monolayers and monolayers overexpressing hBest1 or hBest1^{W93C} after ATP-stimulation, as well as after subsequent washout of ATP. **B**: Prior to ATP stimulation, mean baselines $[Ca^{2+}]_i$ between control and overexpressing monolayers are shown. Differences between monolayers were significant ($p<0.005$ versus controls, n=4). Data are mean ± SEM.

data for bacterial and chicken Best1 [5,6], as well as in vivo neuronal data [22,23], have made it unambiguously clear that Best1 functions as a homo-pentameric anion channel with an ion conductance pore at its center. Moreover, we and others have shown that endogenous hBest1 can be cell-surface biotinylated [7,39], that overexpressed hBest1 in native and heterologous systems can be cell-surface biotinylated [7,24,40-42], that hBest1 co-localizes with the plasma membrane marker MCT-1 when expressed in MDCK cells [43], and that anti-Best1 antibody-labeled gold particles are found at the basal membrane of the RPE in eyes from rhesus monkeys [8]. With this in mind, overexpression of hBest1 in fhRPE should cause an increase in the number of anion channels in the basolateral plasma membrane. This would be theorized to result in an increase in TEP due to a relative depolarization of the basolateral plasma membrane. I_{sc}, which reflects all net ionic fluxes, would also be increased by Best1-enhanced electrogenic anion (e.g., Cl^-) transport. This is very similar to our reported data in Figure 3, where monolayers overexpressing hBest1 showed significantly increased TEP (Figure 3A) and I_{sc} (Figure 3C) compared to controls. A slight reduction in TER was observed, but it did not reach statistical significance (Figure 3B). We have previously shown that hBest1^{W93C} physically interacts with WT hBest1 [32], and we show in Figure 1 that hBest1^{W93C}-YFP dominantly suppresses the Cl^- channel activity of hBest1-CFP (Figure 1C) in HEK293 cells. As such, overexpression of hBest1^{W93C} should physically interact with endogenous hBest1 channels in fhRPE and impair their activity. This loss of basolateral plasma membrane CAACs would be predicted to decrease TEP and I_{sc}. Our data show that overexpression of hBest1^{W93C} significantly decreases TEP (Figure 3A) and I_{sc} (Figure 3C) compared to controls. While

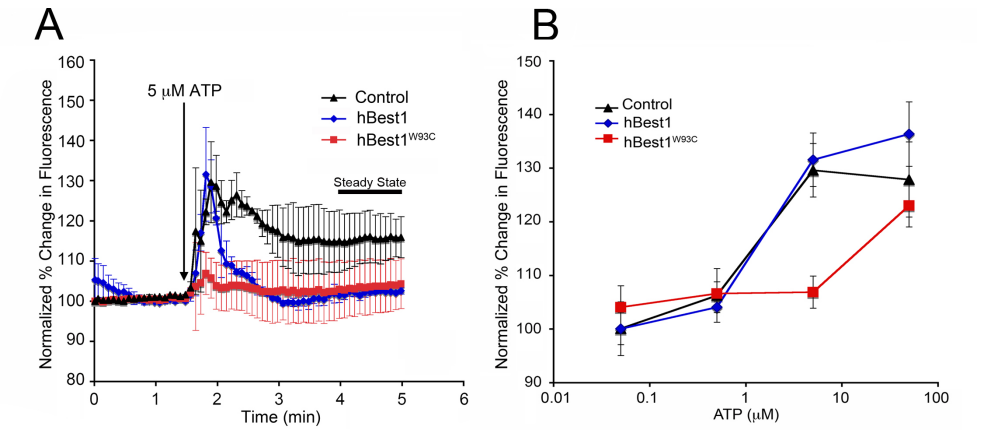

Figure 7. Dose-responsive effect of ATP on $[Ca^{2+}]_i$ in fhRPE cells. **A**: Represented by normalized change in percent fluorescence, the responses in $[Ca^{2+}]$ to 5 µM ATP are shown for control fhRPE and fhRPE overexpressing hBest1 or hBest1^{W93C} **B**: Dose response curves for the initial rise in $[Ca^{2+}]_i$ as a function of ATP concentration are shown for control monolayers and for monolayers overexpressing wild-type or mutant hBest1. ATP doses were between 1 and 100 µM. Differences in responses between each group were significant by ANOVA ($p<0.003$, $n\geq5$). Data are mean ± SEM.

TER remained unchanged (Figure 3B), these observations are analogous to the predicted changes resulting from overexpression or impairment of an anion channel. The lack of significant change in TER may be caused by the compensatory activity of other channels or other confounding factors.

This interpretation is further supported by the gluconate substitution experiment shown in Figure 3E. That no significant change in I_{sc} was observed in monolayers overexpressing Best1^{W93C} following Cl^- substitution (Figure 3E) suggests that the W93C mutation abolishes any Best1-associated Cl^- conductance. For hBest1-overexpressing but not control monolayers, a significant decrease in I_{sc} following gluconate substitution was observed (Figure 3E), suggesting that basolateral Cl^- transport contributed to the increased I_{sc} caused by overexpression of hBest1 (Figure 3C). Data in Figure 4 also support this interpretation for two reasons: 1) NFA reduced TEP and I_{sc} of control and hBest1 monolayers, but not hBest1^{W93C} monolayers. This indicates that the W93C mutation abolishes a function of hBest1 that is sensitive to inhibition by NFA. For control and hBest1-overexpressing monolayers, the reduction in I_{sc} (Figure 4C) and TEP (Figure 4D) in response to NFA was roughly equal to the difference in these parameters between the P1 and P2 time points. Thus, this difference between P2 and P1 may represent the component corresponding specifically to CAAC activation. 2) Despite removing Ca^{2+} influx and altered Ca^{2+} signaling as a variable via the application of ionomycin, TEP and I_{sc} were still reduced in hBest1^{W93C} monolayers. This would suggest that these parameters are being impaired, at least in part, by a malfunction of Best1^{W93C} that is independent on Ca^{2+} signaling. Oddly, the application of NFA decreased TEP and I_{sc} to a comparable extent in both control and hBest1-overexpressing monolayers. This may have been due to the activation of other channels by ionomycin (e.g., another CAAC or the maxi-K^+ Ca^{2+}-dependent K^+ channel).

A second possibility is that that these changes are caused by hBest1-induced regulation of intracellular Ca^{2+} signaling. This could occur via known interaction between Best1 and VDCCs [18], or by a recently proposed subpopulation of Best1 that resides in an internal compartment very near the basolateral plasma membrane [10]. For the latter, Best1 would function as an intracellular Cl^- channel and conduct Cl^- as a counterion for Ca^{2+}, working to help accumulate and release Ca^{2+} from intracellular stores [9-11]. Overexpression of hBest1 caused a faster rise in $[Ca^{2+}]_i$ and a faster release following ATP stimulation (Figure 7A), lending some credence to this theory. These effects on transepithelial electrical properties and Ca^{2+} could have also been mediated by functional and physical interaction with VDCCs. Such interaction has been observed independently by three different laboratories [24-28]. None of these possibilities preclude the other, however, and it is feasible that hBest1 anion channels in the plasma membrane, hBest1 anion channels in an internal compartment adjacent to the plasma membrane, and VDCCs all play a role in mediating the reported changes in transepithelial electrical properties (Figure 3, Figure 4, Figure 5) and intracellular Ca^{2+} signaling (Figure 6 and Figure 7).

In Figure 5, we show that stimulation with ATP differentially affects the transepithelial electrical properties of control, hBest1-overexpressing, and hBest1^{W93C}-overexpressing monolayers. Since ATP stimulation of RPE increases $[Ca^{2+}]_i$, and Best1 is a CAAC, we would have expected ATP application to increase both TEP and I_{sc} in fhRPE monolayers overexpressing hBest1. Instead, we observed a large decrease in both TEP (Figure 5B) and TER (Figure 5C) in these monolayers. The drop in TEP resulted from the drop in TER. This drop is an indicator of a tight junction breakdown. Since Best1 has been reported to regulate and be regulated by volume [44,45], one possibility for this drop in TER is that ATP stimulation following overexpression of hBest1 may have caused cell shrinkage. That this was only observed following ATP stimulation (Figure 5) and not after ionomycin (Figure 4) is interesting, and indicates that increasing $[Ca^{2+}]_i$ via the ATP-specific pathway results in different effects than more broadly increasing Ca^{2+} via application with ionomycin.

Our Ca^{2+} data indicate that resting, baseline $[Ca^{2+}]_i$ is significantly altered by the expression of hBest1 or hBest1^{W93C} (Figure 6B). This indicates that, independent of a signal (e.g., ATP), hBest1 can still exert significant effects on Ca^{2+} homeostasis. We have previously observed an increase in the release of $[Ca^{2+}]_i$ triggered by extracellular ATP in RPE explants from *Best1*$^{-/-}$ mice [20], and complete suppression of ATP-stimulated Ca^{2+} release in the RPE of *Best1*^{W93C} knock-in mice [21]. It is important to note that the ATP-induced release of Ca^{2+} in human RPE, fetal or otherwise, differs from that observed in mouse RPE. Mice lack the fast component of Ca^{2+} release observed in Figure 6 and Figure 7, by Petersen and coworkers [29], and by Singh et al. [12], who used iPSC-derived hRPE cells. In the present study, we show that overexpression of hBest1 or hBest1^{W93C} greatly diminished the sustained increase in cytosolic Ca^{2+} in response to ATP in fhRPE (Figure 6 and Figure 7). However, overexpression of hBest1 did result in a more rapid initial increase in $[Ca^{2+}]_i$ (Figure 6 and Figure 7), and the overall response of monolayers expressing hBest1^{W93C} were impaired compared to control and hBest1-overexpressing monolayers (Figure 6 and Figure 7). While our data for hBest1^{W93C} are similar in mouse and human RPE in that hBest1^{W93C} suppresses Ca^{2+}

release following stimulation with ATP, they differ from that observed by Singh et al. [12] in human iPSC-derived RPE cells for the BVMD associated mutations A146K and N296H. These mutants caused an increase in the fast response more akin to that observed in our study for overexpression of WT hBest1 [12] (Figure 6 and Figure 7). One possible explanation for the difference is that different mutations can either constitutively activate the Ca^{2+} regulatory function of Best1, or alternatively inactivate it. Regardless, in both cases, intracellular Ca^{2+} in response to ATP stimulation is altered by mutations in hBest1, and it is likely that this effect varies with different mutations.

In summary, our data demonstrate that Best1 can influence transepithelial electrical properties and intracellular Ca^{2+} signaling in human RPE. They also provide support for Best1-associated anion channel activity in human RPE. The current data illustrate that mutations in *BEST1* do this detrimentally, suggesting a potential mechanism for the primary defects observed in BVMD: a diminished EOG LP, fluid-filled retinal detachments, and lipofuscin accumulation [1-3,46]. Further studies are required to determine how impairing these functions individually or together contribute to the phenotypes of the different diseases caused by *BEST1* mutations.

ACKNOWLEDGMENTS

This work was funded by grants from the NIH (R01EY13160 to ADM, R01EY13847 to LYM, HL66044 to RML), the Macular Vision Research Foundation (ADM), and unrestricted grants to the Departments of Ophthalmology at the Mayo Clinic and the University of Arizona from Research to Prevent Blindness.

REFERENCES

1. Blodi CF, Stone EM. Best's vitelliform dystrophy. Ophthalmic Paediatr Genet 1990; 11:49-59. [PMID: 2190134].
2. Boon CJ, Klevering BJ, Leroy BP, Hoyng CB, Keunen JE, den Hollander AI. The spectrum of ocular phenotypes caused by mutations in the BEST1 gene. Prog Retin Eye Res 2009; 28:187-205. [PMID: 19375515].
3. Marmorstein AD, Cross HE, Peachey NS. Functional roles of bestrophins in ocular epithelia. Prog Retin Eye Res 2009; 28:206-26. [PMID: 19398034].
4. Pasquay C, Wang LF, Lorenz B, Preising MN. Bestrophin 1 - Phenotypes and Functional Aspects in Bestrophinopathies. Ophthalmic Genet 2013; [PMID: 24328569].
5. Dickson VK, Pedi L, Long SB. Structure and insights into the function of a Ca-activated Cl channel. Nature 2014; .
6. Yang T, Liu Q, Kloss B, Bruni R, Kalathur RC, Guo Y, Kloppmann E, Rost B, Colecraft HM, Hendrickson WA. Structure and selectivity in bestrophin ion channels. Science 2014; 346:355-9. [PMID: 25324390].
7. Marmorstein AD, Marmorstein LY, Rayborn M, Wang X, Hollyfield JG, Petrukhin K. Bestrophin, the product of the Best vitelliform macular dystrophy gene (VMD2), localizes to the basolateral plasma membrane of the retinal pigment epithelium. Proc Natl Acad Sci USA 2000; 97:12758-63. [PMID: 11050159].
8. Gouras P, Braun K, Ivert L, Neuringer M, Mattison JA. Bestrophin detected in the basal membrane of the retinal epithelium and drusen of monkeys with drusenoid maculopathy. Graefes Arch Clin Exp Ophthalmol 2009; 247:1051-6. [PMID: 19421767].
9. Neussert R, Muller C, Milenkovic VM, Strauss O. The presence of bestrophin-1 modulates the Ca2+ recruitment from Ca2+ stores in the ER. Pflugers Arch 2010; 460:163-75. [PMID: 20411394].
10. Strauss O, Muller C, Reichhart N, Tamm ER, Gomez NM. The role of bestrophin-1 in intracellular Ca(2+) signaling. Adv Exp Med Biol 2014; 801:113-9. [PMID: 24664688].
11. Gómez NM, Tamm ER, Straubeta O. Role of bestrophin-1 in store-operated calcium entry in retinal pigment epithelium. Pflugers Arch 2013; 465:481-95. [PMID: 23207577].
12. Singh R, Shen W, Kuai D, Martin JM, Guo X, Smith MA, Perez ET, Phillips MJ, Simonett JM, Wallace KA, Verhoeven AD, Capowski EE, Zhang X, Yin Y, Halbach PJ, Fishman GA, Wright LS, Pattnaik BR, Gamm DM. iPS cell modeling of Best disease: insights into the pathophysiology of an inherited macular degeneration. Hum Mol Genet 2013; 22:593-607. [PMID: 23139242].
13. Cross HE, Bard L. Electro-oculography in Best's macular dystrophy. Am J Ophthalmol 1974; 77:46-50. [PMID: 4824173].
14. Gallemore RP, Steinberg RH. Effects of DIDS on the chick retinal pigment epithelium. II. Mechanism of the light peak and other responses originating at the basal membrane. J Neurosci 1989; 9:1977-84. [PMID: 2723762].
15. Gallemore RP, Steinberg RH. Light-evoked modulation of basolateral membrane Cl- conductance in chick retinal pigment epithelium: the light peak and fast oscillation. J Neurophysiol 1993; 70:1669-80. [PMID: 8283222].
16. Gallemore RPBH, Miller SS. Light-induced responses of the retinal pigment epithelium. In: Marmor MF TW, editor. The retinal pigment epithelium: function and disease. New York: Oxford University Press; 1998. p. 175–98.
17. Hartzell HC, Qu Z, Yu K, Xiao Q, Chien LT. Molecular physiology of bestrophins: multifunctional membrane proteins linked to best disease and other retinopathies. Physiol Rev 2008; 88:639-72. [PMID: 18391176].
18. Xiao Q, Hartzell HC, Yu K. Bestrophins and retinopathies. Pflugers Arch 2010; 460:559-69. [PMID: 20349192].

19. Sun H, Tsunenari T, Yau KW, Nathans J. The vitelliform macular dystrophy protein defines a new family of chloride channels. Proc Natl Acad Sci USA 2002; 99:4008-13. [PMID: 11904445].

20. Marmorstein LY, Wu J, McLaughlin P, Yocom J, Karl MO, Neussert R, Wimmers S, Stanton JB, Gregg RG, Strauss O, Peachey NS, Marmorstein AD. The light peak of the electroretinogram is dependent on voltage-gated calcium channels and antagonized by bestrophin (best-1). J Gen Physiol 2006; 127:577-89. [PMID: 16636205].

21. Zhang Y, Stanton JB, Wu J, Yu K, Hartzell HC, Peachey NS, Marmorstein LY, Marmorstein AD. Suppression of Ca2+ signaling in a mouse model of Best disease. Hum Mol Genet 2010; 19:1108-18. [PMID: 20053664].

22. Lee S, Yoon BE, Berglund K, Oh SJ, Park H, Shin HS, Augustine GJ, Lee CJ. Channel-mediated tonic GABA release from glia. Science 2010; 330:790-6. [PMID: 20929730].

23. Woo DH, Han KS, Shim JW, Yoon BE, Kim E, Bae JY, Oh SJ, Hwang EM, Marmorstein AD, Bae YC, Park JY, Lee CJ. TREK-1 and Best1 channels mediate fast and slow glutamate release in astrocytes upon GPCR activation. Cell 2012; 151:25-40. [PMID: 23021213].

24. Rosenthal R, Bakall B, Kinnick T, Peachey N, Wimmers S, Wadelius C, Marmorstein A, Strauss O. Expression of bestrophin-1, the product of the VMD2 gene, modulates voltage-dependent Ca2+ channels in retinal pigment epithelial cells. FASEB J 2006; 20:178-80. [PMID: 16282372].

25. Yu K, Xiao Q, Cui G, Lee A, Hartzell HC. The best disease-linked Cl- channel hBest1 regulates Ca V 1 (L-type) Ca2+ channels via src-homology-binding domains. J Neurosci 2008; 28:5660-70. [PMID: 18509027].

26. Milenkovic VM, Krejcova S, Reichhart N, Wagner A, Strauss O. Interaction of bestrophin-1 and Ca2+ channel beta-subunits: identification of new binding domains on the bestrophin-1 C-terminus. PLoS ONE 2011; 6:e19364-[PMID: 21559412].

27. Reichhart N, Milenkovic VM, Halsband CA, Cordeiro S, Strauss O. Effect of bestrophin-1 on L-type Ca2+ channel activity depends on the Ca2+ channel beta-subunit. Exp Eye Res 2010; 91:630-9. [PMID: 20696156].

28. Burgess R, Millar ID, Leroy BP, Urquhart JE, Fearon IM, De Baere E, Brown PD, Robson AG, Wright GA, Kestelyn P, Holder GE, Webster AR, Manson FD, Black GC. Biallelic mutation of BEST1 causes a distinct retinopathy in humans. Am J Hum Genet 2008; 82:19-31. [PMID: 18179881].

29. Peterson WM, Meggyesy C, Yu K, Miller SS. Extracellular ATP activates calcium signaling, ion, and fluid transport in retinal pigment epithelium. J Neurosci 1997; 17:2324-37. [PMID: 9065493].

30. Wu J, Marmorstein AD, Striessnig J, Peachey NS. Voltage-dependent calcium channel CaV1.3 subunits regulate the light peak of the electroretinogram. J Neurophysiol 2007; 97:3731-5. [PMID: 17376851].

31. Marmorstein AD, Stanton JB, Yocom J, Bakall B, Schiavone MT, Wadelius C, Marmorstein LY, Peachey NS. A model of best vitelliform macular dystrophy in rats. Invest Ophthalmol Vis Sci 2004; 45:3733-9. [PMID: 15452084].

32. Johnson AA, Lee YS, Stanton JB, Yu K, Hartzell CH, Marmorstein LY, Marmorstein AD. Differential effects of Best disease causing missense mutations on bestrophin-1 trafficking. Hum Mol Genet 2013; 22:4688-97. [PMID: 23825107].

33. Hu J, Bok D. A cell culture medium that supports the differentiation of human retinal pigment epithelium into functionally polarized monolayers. Mol Vis 2001; 7:14-9. [PMID: 11182021].

34. Ablonczy Z, Dahrouj M, Tang PH, Liu Y, Sambamurti K, Marmorstein AD, Crosson CE. Human retinal pigment epithelium cells as functional models for the RPE in vivo. Invest Ophthalmol Vis Sci 2011; 52:8614-20. [PMID: 21960553].

35. Johnson AA, Lee YS, Chadburn AJ, Tammaro P, Manson FD, Marmorstein LY, Marmorstein AD. Disease-causing mutations associated with four bestrophinopathies exhibit disparate effects on the localization, but not the oligomerization, of Bestrophin-1. Exp Eye Res 2014; 121:74-85. [PMID: 24560797].

36. Oakley B 2nd, Steinberg RH, Miller SS, Nilsson SE. The in vitro frog pigment epithelial cell hyperpolarization in response to light. Invest Ophthalmol Vis Sci 1977; 16:771-4. [PMID: 885686].

37. Miller SS, Steinberg RH. Passive ionic properties of frog retinal pigment epithelium. J Membr Biol 1977; 36:337-72. [PMID: 302862].

38. Grynkiewicz G, Poenie M, Tsien RY. A new generation of Ca2+ indicators with greatly improved fluorescence properties. J Biol Chem 1985; 260:3440-50. [PMID: 3838314].

39. Brandl C, Zimmermann SJ, Milenkovic VM, Rosendahl SM, Grassmann F, Milenkovic A, Hehr U, Federlin M, Wetzel CH, Helbig H, Weber BH. In-depth characterisation of Retinal Pigment Epithelium (RPE) cells derived from human induced pluripotent stem cells (hiPSC). Neuromolecular Med 2014; 16:551-64. [PMID: 24801942].

40. Yu K, Cui Y, Hartzell HC. The bestrophin mutation A243V, linked to adult-onset vitelliform macular dystrophy, impairs its chloride channel function. Invest Ophthalmol Vis Sci 2006; 47:4956-61. [PMID: 17065513].

41. Yu K, Qu Z, Cui Y, Hartzell HC. Chloride channel activity of bestrophin mutants associated with mild or late-onset macular degeneration. Invest Ophthalmol Vis Sci 2007; 48:4694-705. [PMID: 17898294].

42. Doumanov JA, Zeitz C, Dominguez Gimenez P, Audo I, Krishna A, Alfano G, Diaz ML, Moskova-Doumanova V, Lancelot ME, Sahel JA, Nandrot EF, Bhattacharya SS. Disease-causing mutations in BEST1 gene are associated with altered sorting of bestrophin-1 protein. Int J Mol Sci 2013; 14:15121-40. [PMID: 23880862].

43. Milenkovic VM, Rohrl E, Weber BH, Strauss O. Disease-associated missense mutations in bestrophin-1 affect cellular trafficking and anion conductance. J Cell Sci 2011; 124:2988-96. [PMID: 21878505].

44. Chien LT, Hartzell HC. Drosophila bestrophin-1 chloride current is dually regulated by calcium and cell volume. J Gen Physiol 2007; 130:513-24. [PMID: 17968025].

45. Stotz SC, Clapham DE. Anion-sensitive fluorophore identifies the Drosophila swell-activated chloride channel in a genome-wide RNA interference screen. PLoS ONE 2012; 7:e46865-[PMID: 23056495].

46. Bakall B, Radu RA, Stanton JB, Burke JM, McKay BS, Wadelius C, Mullins RF, Stone EM, Travis GH, Marmorstein AD. Enhanced accumulation of A2E in individuals homozygous or heterozygous for mutations in BEST1 (VMD2). Exp Eye Res 2007; 85:34-43. [PMID: 17477921].

Articles are provided courtesy of Emory University and the Zhongshan Ophthalmic Center, Sun Yat-sen University, P.R. China. The print version of this article was created on 1 April 2015. This reflects all typographical corrections and errata to the article through that date. Details of any changes may be found in the online version of the article.